Fluidization of Nanoagglomerates in a Rotating Fluidized Bed

Jose Quevedo and Robert Pfeffer
Dept. of Chemical Engineering, New Jersey Institute of Technology, Newark, NJ 07102

Yueyang Shen and Rajesh Dave
Dept. of Mechanical Engineering, New Jersey Institute of Technology, Newark, NJ 07102

Hideya Nakamura and Satoru Watano
Dept. of Chemical Engineering, Osaka Prefecture University, 1-1 Gakuen-cho, Sakai, Osaka 5998531, Japan

DOI 10.1002/aic.10826
Published online April 13, 2006 in Wiley InterScience (www.interscience.wiley.com).

Agglomerates of nanoparticles were fluidized in a rotating fluidized bed (RFB) system at different rotating speeds corresponding to 10, 20, 30 and 40 times the gravity force (9.8 m/s^2). The powders, fumed silica Aerosil® R974, Aerosil® R972 and Aeroxide® TiO_2 P25, with a primary particle size of 12, 16 and 21 nm, respectively, form micron sized nanoagglomerates having a very low bulk density of around 30 kg/m^3 for the fumed silicas, and a somewhat higher bulk density of about 90 kg/m^3 for Aeroxide® TiO_2 P25. Their fluidization behaviors are described by the fluidized bed expansion, pressure drop and minimum fluidization velocity (U_{mf}). It was found that the fumed silica agglomerates expanded considerably while the TiO_2 agglomerates showed very little bed expansion. The minimum fluidization velocities for Aerosil® R974 and R972 ranged from 0.02 to 0.07 m/s and from 0.13 to 0.20 m/s for Aeroxide® TiO_2 P25; U_{mf} increased at higher rotating speeds for all powders.

At gas velocities above U_{mf}, the fluidized bed pressure drop of fumed silica agglomerates was higher than theoretically estimated by mathematical models found in the literature. Thus, it is believed that for these light particles additional tangential momentum effects may increase the bed pressure drop and a revised model is proposed. In addition, the agglomerate size and external void fraction of the bed are predicted by using a fractal analysis coupled with a modified Richardson-Zaki equation for data obtained with Aerosil® R972. © 2006 American Institute of Chemical Engineers *AIChE J,* 52: 2401–2412, 2006

Keywords: fluidization, rotating fluidized bed, centrifugal force, nanoparticles, nanoagglomerates, coriolis force

Introduction

Because of their unique properties due to their very small primary particle size and very large surface area per unit mass, nanostructured materials are already being used in the manufacture of drugs, cosmetics, foods, plastics, catalysts, and energetic and biomaterials. Therefore, it is necessary to develop processing technologies, which can handle large quantities of nanosized particles, for example, mixing, transporting, modifying the surface properties (coating),[1, 2] and downstream processing of nanoparticles to form nanocomposites. However, before processing of nanostructured materials can take place, the nanosized particles have to be well dispersed. Gas fluidization is one of the best techniques available to disperse and process powders, and is widely used in a variety of industrial

Correspondence concerning this article should be addressed to R. N. Dave at dave@adm.njit.edu.

applications because of its capability of continuous powder handling, good mixing, large gas-solid contact area and very high rates of heat and mass transfer, and is one of the best techniques available to disperse and process powders. Moreover, it has been demonstrated that a rotating fluidizing bed (RFB) system has advantages over conventional fluidized beds in terms of handling of very fine powders due to the additional forces generated by the rotation of the assembly.[3]

To date, several studies on fluidization of agglomerates of nanoparticles have been done which include conventional fluidization[4] and externally assisted fluidization involving the use of additional forces generated by vibratory,[5] acoustic,[6] or magnetic fields[7] to enhance the dynamics of the powder in the fluidized bed. It also has been found that the nanoparticles form fractal agglomerates,[5] and that the size and porosity of the agglomerates affect the nature of fluidization; therefore, several studies have focused on theoretical predictions of the average agglomerate size,[4, 5] as well as altering its size by external excitations.[3-7]

Wang et al.[8] found that when fluidizing different nanoparticles, the fluidization behavior can be classified as either agglomerate particulate fluidization (APF) or agglomerate bubbling fluidization (ABF). APF is characterized by a large bed expansion of up to three to five times the original bed height, smooth fluidization and very low minimum fluidization velocities. ABF shows little bed expansion, bubbling, and the bed behaves more like Geldart group B micron size particles. This is in agreement with the fluidization behavior observed by Zhu et al.[4] where some nanoparticles fluidized homogeneously (APF), and others formed large bubbles and channels (ABF).

Among the several studies on rotating fluidized beds, Kroger et al.[9] estimated the bed pressure drop and flow distribution in both packed and fluidized rotating beds of spherical particles. In a section of their modeling work, they analyzed how the tangential velocity and effective viscosity of the fluidized bed could affect the pressure drop in a fluidized bed. They concluded that in some cases a decrease in the effective viscosity caused by an increase in void fraction could lead to tangential momentum effects within the fluidized bed which would increase its pressure drop; we believe that this phenomenon also occurs while fluidizing APF agglomerates of nanoparticles, although it should be noted that the modeling done by Kroger et al.[9] did not consider nanoparticles.

By fluidizing micron size alumina particles and glass beads, Qian et al.[3] concluded that the fluidization behavior of fine particles can be changed from Geldart group C to Geldart group A due to the centrifugal acceleration, the value of which could be adjusted to several times the acceleration of gravity by simply increasing the rotating speed of the distributor. Kao et al.[10] developed equations for predicting the pressure drop and the minimum fluidization velocity of a fluidized bed of mm size particles. They simplified the equations previously developed by Chen[11], who for modeling purposes assumed that the fluidized bed rotated like a rigid body. Chen[11] also suggested that in a rotating-fluidized bed, the particulate material is fluidized layer by layer from the solid-gas interface outward at increasing radius as the gas velocity is increased. The phenomenon of fluidization, layer by layer, which is caused by the radial velocity being higher and the centrifugal force lower at the bed's interface, is useful to explain the fact that the bed void fraction at the bed's interface, that is, the freeboard region, is lower than the bed void fraction in the proximity of the distributor.

Extensive modeling and numerical simulations of the flow pattern in a rotating cylinder containing a packed bed was done by Arman[12]. His work describes the different flow regions inside the rotating cylinder that arise as a consequence of the type of flow. He also describes the presence of a significant tangential velocity of the fluid gas right above the packed bed or fluidized bed of particles; this is important for explaining the additional tangential momentum effects that can alter the bed pressure drop.

Watano et al. granulated particles of cornstarch (about 15 microns in size) using an RFB unit,[13] showing the potential applications of this device for the pharmaceutical industry. Saunders'[14] study on the entrainment of particles coming from an RFB, explained the importance of the ratio of fluidizing velocity to particle terminal velocity at the surface of the rotating bed.

Recently, Matsuda et al.[15] fluidized agglomerates of nanoparticles of TiO_2 with a primary particle size of 7 nm, which is smaller in size than the nanosized TiO_2 fluidized in this work. They presented a model based on an energy balance which predicts a reduction in agglomerate size at higher centrifugal forces. However, the agglomerate sizes used to validate the model were obtained by measuring minimum fluidization velocities and using correlations from Wen and Yu[16], rather than by direct agglomerate size measurements. They concluded that the agglomerate size was reduced at higher centrifugal accelerations.

In this work, nanoparticles agglomerates of fumed silica, namely, Aerosil® R974 and Aerosil® R972 (provided by Degussa Japan - Nippon Aerosil Co.), and Aeroxide® Titanium Dioxide P25 (provided by Degussa Corp. USA) were fluidized while subject to 10, 20, 30 and 40 times normal gravity acceleration. Data, such as the fluidized-bed height and pressure drop were recorded and used to approximate the minimum fluidization velocity by plotting the bed pressure drop against the gas velocity.

In conventional fluidization, Aerosil® R974 and Aerosil® R972 show an agglomerate particulate fluidization (APF) behavior, which is characterized by a bed expansion of about several times the initial bed height depending on the gas velocity.[4-8] It has been found in this work that in an RFB, the initial bed height is almost doubled during fluidization of these powders, and that the fluidized bed pressure drop is higher than that theoretically estimated by Kao's model.[10]

It is believed that the effective viscosity and the Darcy number of the fluidized bed are significantly reduced due to the large total bed void fraction; thus, the tangential velocity component of the gas flow within the fluidized bed may become significant, in particular, in the vicinity of the gas-solid interface. As a result, the fluidized bed pressure drop may increase due to additional forces caused by the tangential momentum effects. The influence of the tangential gas motion, when fluidizing APF nanoagglomerates, is a major focus of the current article.

Experimental Method

Details of the rotating fluidized bed unit, customized by Nara Machinery Co. (Tokyo, Japan), are shown in Figure 1. It

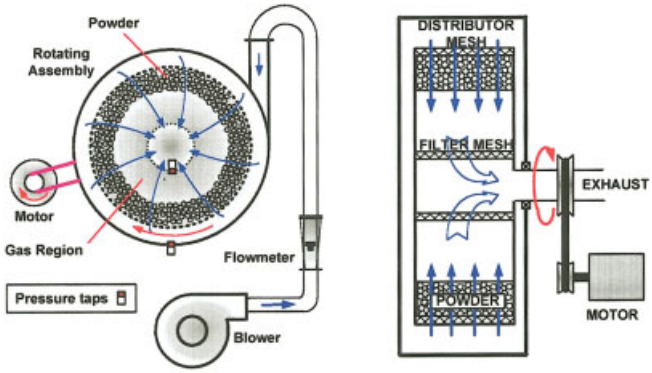

Figure 1. Rotating fluidized-bed unit.

[Color figure can be viewed in the online issue, which is available at www.interscience.wiley.com.]

consists of an air-pressurized chamber, which encloses a cylindrical stainless steel sintered mesh with a dia. of 400 mm, and a depth of 100 mm. This 2 mm thick mesh has apertures of 20 microns and acts as the gas distributor, it rotates along its horizontally directed axis of symmetry and its angular velocity, measured by a tachometer, can be adjusted by a variable speed electric motor. The fluidization behavior can be observed because the frontal covers of the pressurized chamber and the rotating air distributor are made of translucent acrylic plastic.

A blower (Hitachi VBD-080), driven by a variable speed electric motor, delivers air to the chamber; the flow of air is measured with a variable area type flowmeter. Pressure taps are placed as shown in Figure 1 in such a way that the pressure drop is measured along the radial direction; a differential pressure transmitter is connected to the taps and linked to a computer for recording data. In addition, a digital camera is used to record the fluidization of the agglomerates of nanoparticles and a laser-pointer is used to measure the bed height and to see the surface of the fluidized bed. Further details of the rotating fluidized bed unit can be found in Watano et al.[13]

Under normal gravity conditions, that is, conventional fluidization, Aerosil® R974 and R972 fluidize smoothly, which is characteristic of agglomerate particulate fluidization (APF);[17] on the other hand, Aeroxide® TiO_2 P25 fluidizes with the presence of bubbles and a irregular bed surface, typical of an agglomerate bubbling fluidization (ABF) behavior.[17] These powders are quite different than Geldart group C powders because they consist of highly porous agglomerates; as a result, the bulk density of these powders is much lower than the bulk density of micron size powders.[4-7]

Due to the relatively long period of time that the nanoparticles are stored and/or transported before using, agglomerates of different sizes form because of consolidation due to the cohesive interactions between the nanoparticles, that is, densification. Therefore, the powders were sieved using a shaker and a 60 Mesh sieve (mesh opening about 250 um) to discard large agglomerates and for repeatability purposes; this procedure was followed since it was observed that the presence of large agglomerates changes the fluidization behavior. Furthermore, fluidization experiments performed with nonsieved agglomerates did not show good bed expansion (data not shown). These observations are also consistent with the observations reported in Zhu et al.[4] for conventional fluidization.

Fumed silica, Aerosil®, has a tapped density of about 50 g/L (source, Degussa Corp.), and the average primary particle sizes for Aerosil® R974 and R972 are 12 and 16 nanometers, respectively. The bulk density, found experimentally, for both powders was about 30 g/L; 70 g of powder were used in each experimental run. Aeroxide® TiO_2 P25 has an average particle size of 21 nanometers, a tapped density of 130 g/L and a bulk density of about 90 g/L; 250 g of this powder were used in each experiment. In all experiments the initial bed height was about 0.02 meters.

For each different nanopowder, the experimental procedure can be summarized as follows. For a particular rotating speed (set centrifugal force) the air distributor mesh's pressure drop was measured as the air flow rate was gradually increased before loading any powder into the unit, that is, for an empty distributor. The rotating speed was then increased to the next level and the procedure repeated; this was done to obtain the pressure drop across the air distributor as a function of the air flow at different rotational speeds.

The angular speeds selected for the experiments were 22, 31, 38 and 44 rad/s that correspond to centrifugal accelerations of 10, 20, 30 and 40 times gravity acceleration, respectively. A weighed batch of powder was then loaded into the unit, the rotating speed was set, and the air flow was gradually increased in order to record data, such as air flow, pressure drop and bed height. A similar procedure was followed for each angular velocity. The fluidized bed pressure drop was obtained by subtracting the distributor's pressure drop from the pressure drop measured when the unit was loaded with powder at the same flow rate and rotating speed.

Results and discussion

Figures 2, 3 and 4 show the fluidized-bed pressure drop as a function of radial air velocity at the four different centrifugal accelerations for Aerosil® R974, R972 and Aeroxide® TiO_2 P25, respectively. In general, the pressure drop increases until the minimum fluidization velocity is reached, then an approximately constant pressure drop is observed. In some cases, it was not possible to measure the pressure drop at very low-gas velocities, and the pressure drop did not maintain a linear trend before reaching U_{mf} probably due to the instability of the nonfully fluidized bed. It was observed that the fluidized-bed

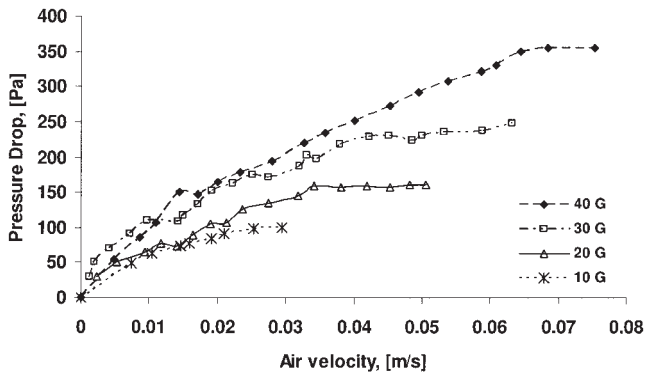

Figure 2. Bed pressure drop of Aerosil® R974 vs. air velocity at different centrifugal accelerations (1 G = 9.8 m/s^2).

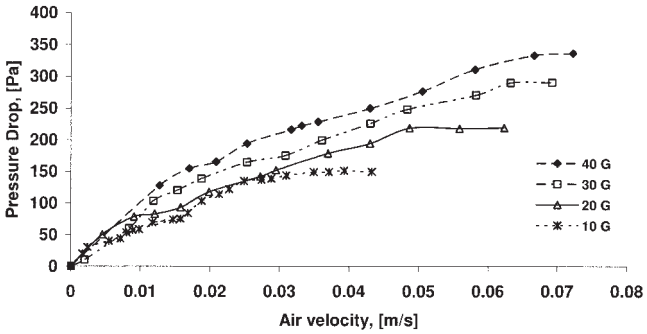

Figure 3. Bed pressure drop of Aerosil® R972 vs. air velocity at different centrifugal accelerations (1 G = 9.8 m/s^2).

pressure drop could be affected by entrainment of powder at gas velocities higher than the minimum fluidization velocity and also, as will be explained below, due to the presence of tangential momentum effects that may increase the fluidized-bed pressure drop.

The values of the minimum fluidization velocities (U_{mf}) at different rotating speeds are obtained from Figures 2, 3 and 4 by selecting the air radial velocity at which the pressure drops becomes constant and plotted against the centrifugal acceleration in terms of artificial gravity, G. As seen in Figure 5, the minimum fluidization velocities appear to be proportional to the centrifugal acceleration in the range from 10 to 40 Gs. However, this linear relationship between the U_{mf} and the centrifugal acceleration fails if we include the minimum fluidization velocity at 1 G (open symbols in Figure 5) obtained during fluidization of the powders in a conventional fluidized bed. The linear relationship may also not hold for higher rotational speeds as shown by the results of Matsuda et al.[15] at 81.5 G. However, the linear relationship in the range of 10 to 40 G was also found by Watano et al.[1] and Qian et al.[3] in their RFB experiments using solid micron sized particles.

Unlike in a conventional gravity-driven fluidized bed, the relationship between the minimum fluidization velocity and the centrifugal force can also be affected by the geometry of the RFB unit since the intensity of the tangential momentum effects depends, among other things, on the existence of a well

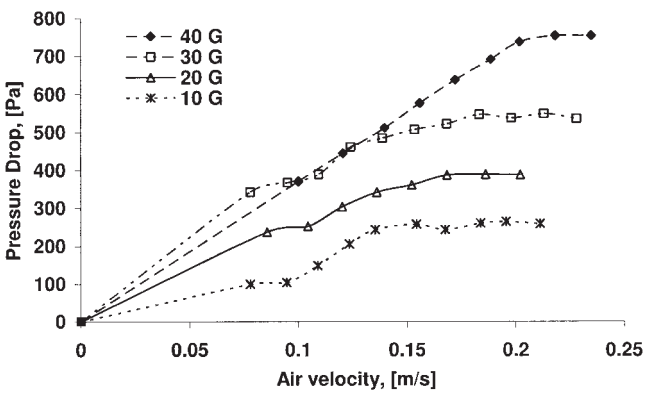

Figure 4. Bed pressure drop of Aeroxide® TiO_2 P25 vs. air velocity at different centrifugal accelerations (1 G = 9.8 m/s^2).

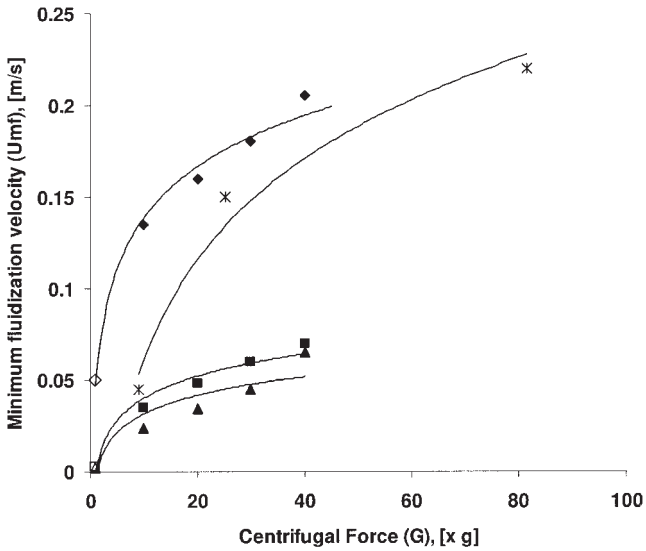

Figure 5. Minimum fluidization velocities of the powders at different rotating speeds (G).

The open symbols are U_{mf} data obtained for these powders in a conventional fluidized bed (Zhu et al.[4]).

developed vortex flow in the freeboard region. Therefore, a plot of the minimum fluidization velocity against the centrifugal force may show different tendencies depending on the nature of the powder, the geometry of the unit and the range of the centrifugal force. For all of these reasons, more research needs to be done to elucidate the relationship between the U_{mf} and the centrifugal force.

The nondimensional fluidized bed height, actual bed height divided by initial bed height, plotted against air velocity at different values of centrifugal force are shown in Figures 6, 7 and 8 for Aerosil® R974, R972 and Aeroxide® TiO_2 P25, respectively. There is a significant bed expansion when fluidizing type APF agglomerates of nanoparticles (R974 and R972) that is almost double the initial bed height at air velocity values slightly higher than the minimum fluidization velocity. The stepwise changes seen in Figures 6 and 7 are probably due to inaccuracies in measuring the bed height at different velocities since this was done with a scale rather than using an automated sensor. Entrainment of powder takes place if the airflow is

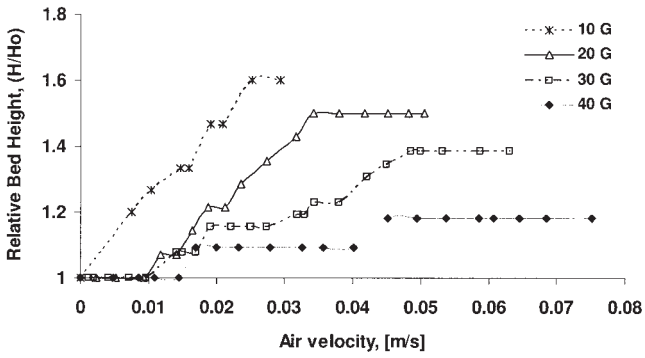

Figure 6. Relative bed height of Aerosil® R974 vs. air velocity observed during fluidization at different centrifugal accelerations (1 G = 9.8 m/s^2).

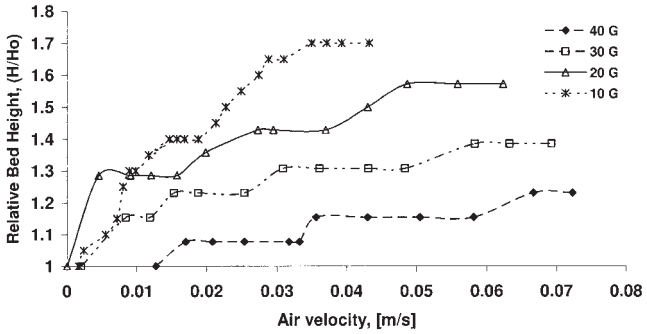

Figure 7. Relative bed height of Aerosil® R972 vs. air velocity observed during fluidization at different centrifugal accelerations (1 G = 9.8 m/s^2).

further increased, which changes the bed pressure drop readings. In the case of Aeroxide® TiO_2 P25, an ABF type powder, the bed expansion was very small and entrainment was also less when compared to the APF type nanopowders.

Furthermore, it was observed that the fluidized bed expansion reduces due to the higher centrifugal force when the rotating speed is increased. It is noted that, unlike R974 and R972 for which the bed expansion is a strong sign of the fully fluidized state, the bed expansion of the TiO_2 P25 is poor giving little clue about its fluidization state, and one must rely solely on the pressure drop data to infer anything about its fluidization behavior.

Experimental measurements of fluidized bed pressure drop at air radial velocities higher than the minimum fluidization velocities are compared against theoretical calculations using the equations presented by Kao et al.[10]. Figure 9a shows that the experimental bed pressure drop values for APF type powders, R974 and R972, are higher than the theoretically calculated values. On the other hand, Figure 9b shows that the experimental bed pressure drops of Aeroxide® TiO_2 P25, an ABF type powder, are close to (or below) the theoretical calculations, and are in general agreement with the results reported by Matsuda et al.[15] who found fluidized bed pressure

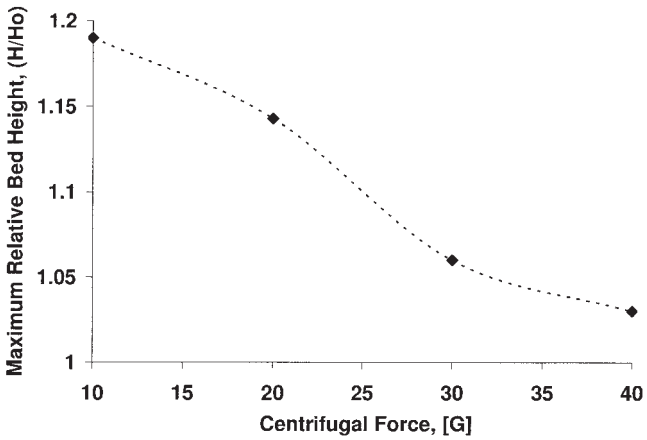

Figure 8. Relative bed height of Aeroxide® TiO_2 P25 vs. air velocity observed during fluidization at different centrifugal accelerations (1 G = 9.8 m/s^2).

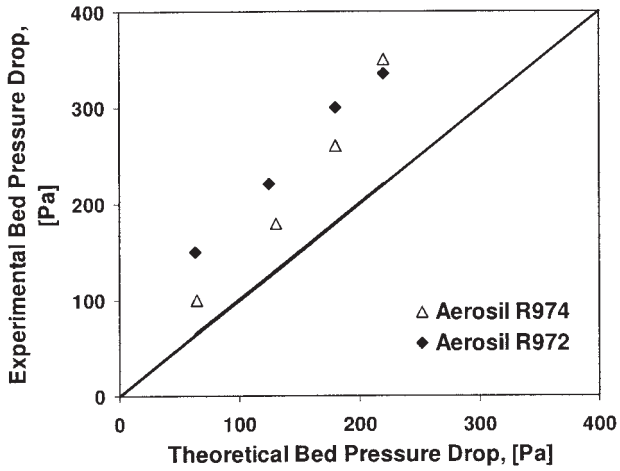

(a)

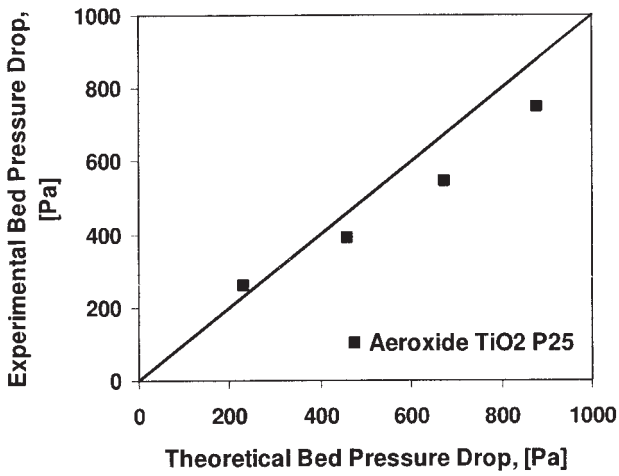

(b)

Figure 9. Experimental data (dots) of the fluidized bed pressure drop at gas velocities higher than the minimum fluidization velocity against the theoretical estimation using Kao's model.

(a) Agglomerates of nanoparticles APF type (Aerosil® R974 and R972), and (b) agglomerates of nanoparticles ABF type (Aeroxide® TiO_2 P25)

drops of TiO_2 to be lower than the theoretical values due to some loss of particles during the experiments.

The dissimilarity between the experimental bed pressure drops of APF and ABF type powders can be explained by the fact that the bed expansion of APF type powders (R974 & R972) is much larger than for ABF powders (TiO_2 P25); moreover, this significant bed expansion is not seen during fluidization of micron size powders. The additional bed expansion means an increase in the void space within the fluidized bed; therefore, it is believed that the high tangential flow of air from the region above the fluidized bed, that is, freeboard-surface interface, can extend into the fluidized bed close to the

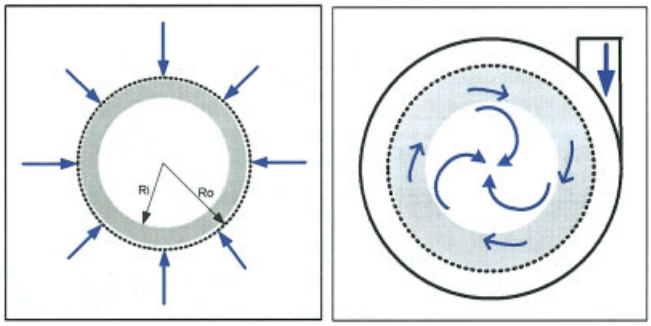

Figure 10. Comparison between the modeling of the flow in a RFB: (a) schematic according to Chen[11] in which a rigid body rotation is assumed for the fluidized bed, valid for modeling micron size and ABF type particles; and (b) when fluidizing APF agglomerates of nanoparticles.

Light gray represents the expanded fluidized bed and the blue arrows stand for the flow of air in the RFB. [Color figure can be viewed in the online issue, which is available at www.interscience.wiley.com.]

interface as shown in Figure 10b, resulting in additional tangential momentum effects[9]; this phenomenon is explained more in detail in the next section.

Flow regime in the RFB when fluidizing nanoparticles

When performing numerical simulations on the flow pattern in a rotating cylinder, Arman[12] described in detail the several flow regions inside of an RFB unit. Furthermore, he performed calculations on a rotating packed bed and he found that the radial velocity component is important within the bed while the tangential velocity component is significant in the region right above of it[12]; in addition, he also found that the tangential velocity within the bed increased as the porosity of the bed increases.

In an RFB, an increase in void fraction within the fluidized bed decreases its effective viscosity, and if the porosity is large enough, the fluidized-bed pressure drop will be increased due to the tangential effects produced by the extension of the tangential flow of the gas from the region above the fluidized bed into it.[9] Since the fluidized bed total void fraction of APF type agglomerates of nanoparticles, before and during fluidization, is larger than the total void fraction of any other class of fluidized powder,, it is possible for the fluid gas to have a significant tangential velocity component within the fluidized bed. In addition, the very low minimum fluidization velocity observed during conventional fluidization of silica nanoagglomerates[4, 17] indicates that these agglomerates are fluffy and light; therefore, a low terminal velocity is expected meaning that these agglomerates can be easily entrained in the direction of the fluid flow, that is, radially and/or tangentially.

A description of the fluid flow in an empty rotating cylinder gives a better understanding of the system. Equation 1 is the nondimensional form of the Navier-Stokes equation for the motion of the fluid inside of a rotating cylinder considering a rotating frame of reference[18, 19]

$$R_o(\vec{\mathbf{u}}\cdot\vec{\nabla})\vec{\mathbf{u}} + 2\vec{\mathbf{k}}\times\vec{\mathbf{u}} = -\vec{\nabla}\mathbf{p} + E_k\nabla^2\vec{\mathbf{u}} \tag{1}$$

and the nondimensional pressure includes the effect of the centrifugal force

$$\nabla\mathbf{p} = \nabla\left[\mathbf{p}^* + \rho\mathbf{\Phi} - \frac{1}{2}\rho(\mathbf{\Omega}\times\mathbf{r})\cdot(\mathbf{\Omega}\times\mathbf{r})\right] \tag{2}$$

where R_o and E_k represent the Rossby and Ekman nondimensional numbers

$$R_o = \frac{U}{\Omega L} = \frac{U}{\Omega R} \tag{3}$$

$$E_k = \frac{\upsilon}{\Omega L^2} = \frac{\upsilon}{\Omega W^2} \tag{4}$$

and U is the fluid velocity, Ω is the rotational speed, ν is the kinematic viscosity, and L describes a geometric length scale related to the fluid flow analysis.

The Rossby and Ekman numbers determine the flow regime within the RFB system; there are five possibilities,[12, 20] linear flow ($1 \gg E_k^{1/4} \gg Ro$), weakly linear flow ($1 \gg E_k^{1/4} > Ro \sim E_k^{1/2}$), weakly nonlinear flow ($1 \gg E_k^{1/4} \sim Ro$), nonlinear flow ($1 \geq Ro \gg E_k^{1/4}$) and turbulent flow ($Ro > 1 \gg E_k^{1/4}$). As mentioned previously, it is important to note that the geometry of the chamber, that is, the radius and width of the rotating distributor, can change the flow regime because the Rossby and Ekman numbers depend on the dimensions of the chamber.

Based on the Rossby and Ekman numbers (Table 1) calculated using our experimental conditions when fluidizing agglomerates of nanoparticles, the flow regime in our experiments can be classified as weakly nonlinear. Therefore, the fluid flow in the empty chamber will be dominated by the tangential velocity component. Similarly, when the unit is loaded with powder, the tangential velocity, will also dominate the freeboard region (above the fluidized bed).

Computational simulations of an empty rotating cylinder

The fact that the flow pattern of air inside of a rotating cylinder is different than a rigid body rotation can be demonstrated by performing simulations using Fluent 6.1. The simulation region was set up in accord with the dimensions of the experimental apparatus; the gas media properties used were those of air. Since the gas speed is relatively high inside the computational field, it is treated as a compressible media instead of incompressible. The standard ***κ-ε*** *turbulence model* is used to describe the turbulent behavior of the gas.

Figure 11a,b,c show the velocity profiles of the fluid (gas) inside of the RFB unit as calculated by Fluent®. The simulations were run by changing the gas velocity at the inlet of the chamber while keeping the rotating speed constant at 211 rpm (10 times the gravity force). The simulations show that the tangential velocity component is highly dependant on the air velocity at the inlet of the chamber; additional simulations run at 411 rpm (40 times gravity force) indicated that the flow was also dependent on the rotating speed of the distributor. From

Table 1. Estimated Values of the Dimensionless Numbers of Gas Flowing Through the Bed during Fluidization of APF Powders

Porosity (epsilon)	Gas Velocity (m/s)	Angular Speed (rad/s)	Centrifugal Acceleration (1g = 9.8 m/s^2)	Non-dimensional numbers			
				Rossby	Ekman	Darcy	Forcheimmer
0.3	0.05	22	10 g	1.E-02	2.E-05	368894	445
0.4	0.05	22	10 g	1.E-02	2.E-05	114338	161
0.5	0.05	22	10 g	1.E-02	2.E-05	40654	69
0.6	0.05	22	10 g	1.E-02	2.E-05	15057	32
0.7	0.05	22	10 g	1.E-02	2.E-05	5334	15
0.8	0.05	22	10 g	1.E-02	2.E-05	1588	7
0.9	0.05	22	10 g	1.E-02	2.E-05	279	2
0.98	0.05	22	10 g	1.E-02	2.E-05	9	0
0.3	0.05	44	40 g	6.E-03	9.E-06	184447	222
0.4	0.05	44	40 g	6.E-03	9.E-06	57169	80
0.5	0.05	44	40 g	6.E-03	9.E-06	20327	34
0.6	0.05	44	40 g	6.E-03	9.E-06	7528	16
0.7	0.05	44	40 g	6.E-03	9.E-06	2667	8
0.8	0.05	44	40 g	6.E-03	9.E-06	794	3
0.9	0.05	44	40 g	6.E-03	9.E-06	139	1
0.98	0.05	44	40 g	6.E-03	9.E-06	4	0

Average particle diameter assumed to be 80 μm.

the simulations, it can be concluded that the fluid velocity in the chamber is mostly tangential, that is, vortex like, and that the velocity increases as the flow of air to the chamber is increased. Thus, the fluid flow in an RFB is far from being like a rigid body rotation. The dependence of the tangential velocity on the gas flow fed to the RFB chamber was verified experimentally by placing flags inside the chamber. At a constant rotating speed of the distributor, the flags bended more as the flow to the chamber was increased. The bending of the flags occurred due to the increase in the drag force because of higher tangential velocities.

Figure 12 shows the simulated tangential velocity of the fluid considering the rotating frame as reference; these values were obtained by subtracting the tangential velocity of the frame (rigid body, Ωr) from the contours of velocity obtained from the results shown in Figure 11. Figure 12 clearly shows how the tangential velocity of the fluid increases due to the change in the inlet velocity. The abscissa represents the radial distance from the center of the chamber in meters such that the distributor is located at 0.2 meters from the center of the chamber (right extreme); while the ordinate gives the values of the velocity of the fluid, mostly tangential. It is important to note that while the radial velocity at the distributor is in the range of 0.01 to 0.1 m/s, the corresponding tangential velocity has values in the range of 1 to 5 m/s, which means that the tangential velocity is at least an order of magnitude larger than the radial velocity.

Tangential momentum effects

Considering the fluid flow within a rotating packed bed, Arman's simulation results[12] show that the radial velocity component dominates the fluid flow pattern within a packed bed of large particles (about 1000 μm) held inside a rotating cylinder; indicating that the tangential velocity component is negligible within a bed of large particles. His conclusions are in agreement with several experimental results on fluidization of several hundred microns or millimeter size particles in an RFB. Kroger et al.[9] further explained that in fluidization of large size particles (larger than 500 um), the fluidized bed rotates like a

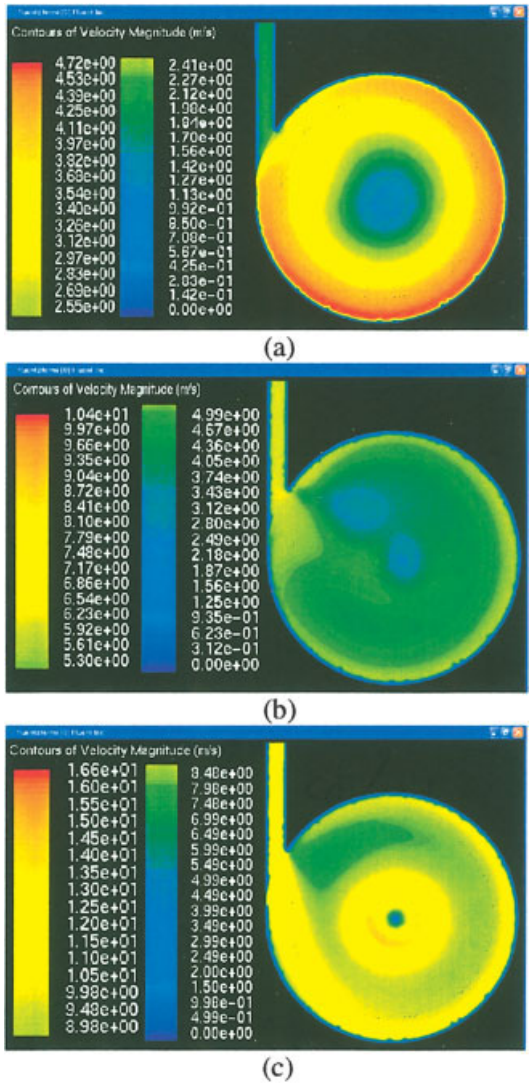

Figure 11. Contours of velocity magnitude of the air inside the rotating cylinder; velocity mostly tangential.

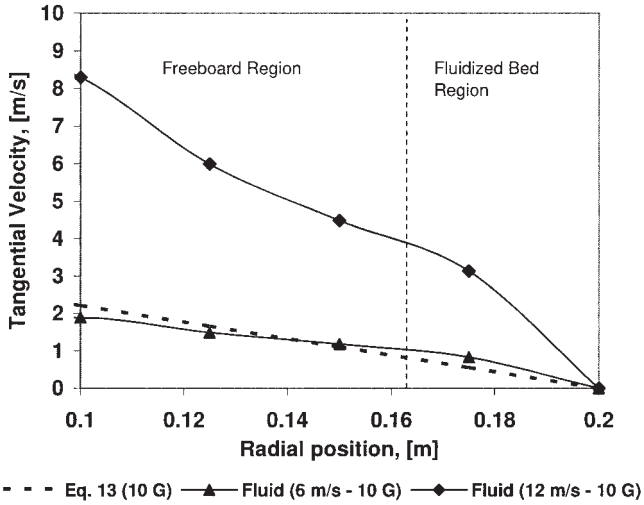

Figure 12. Tangential velocities of the fluid with respect to the rotating frame as function of the radial position in chamber.

Solid lines correspond to the results from the numerical simulations from Figure 11 and the dotted line corresponds to Eq. 14. The vertical dotted line separates the fluidized-bed region from the freeboard.

solid body because of the large effective viscosity (μ_e). However, Kroger[9] concluded that the tangential velocity component within the bed is dependant on the effective viscosity (μ_e); therefore, for low values of the effective viscosity, the tangential velocity component within the bed would become significant and it would increase the pressure drop across the bed.

The effective viscosity is strongly affected by the size of the particles; the larger the diameter of the solids, the higher the effective viscosity, as indicated by Kunii and Levenspiel[21]. The effective viscosity also decreases when the porosity of the bed increases[22]; for example, at gas velocities higher than the minimum fluidization velocity[21, 22, 23] when the bed expands. Thus, the effective viscosity of a fluidized bed of APF type agglomerates of nanoparticles, characterized by a significant bed expansion, should be much lower than the effective viscosity of a bed of solid micron size particles. Kroger et al.[9] concluded that the tangential velocity is related to the effective viscosity in such a way that if the effective viscosity is large, as for a bed of micron or larger size particles, the tangential velocity profile of the bed is similar to a solid body rotation ($v_\theta = \Omega r$); on the other hand, if the effective viscosity is small, approaching to zero, then the tangential velocity profile is similar to a free vortex ($v_\theta = C(r_0/r)$).

Furthermore, Arman[12] concluded that for a rotating fluidized bed, the equation for the radial dependant tangential velocity considering a fixed frame of reference is related to the void fraction of the bed, represented by its permeability, which is included in the Darcy number (D) as shown in the following equation

$$V_\theta = \Omega r + \frac{2|v_{r0}|}{D} \frac{1}{1 + \frac{r}{r_0}} \tag{5}$$

where r_0 is the distributor radius, v_{r0} is the radial velocity passing through the distributor and D is the Darcy nondimensional number

$$D = \frac{v}{\Omega \kappa} \tag{6}$$

where ν is the kinematic viscosity of the fluid and k the permeability.

The total fluidized bed void fraction can be calculated by several correlations; for example, using the equation given by Kroger[9]

$$\rho_s(1 - \varepsilon) = \frac{M_{sh}}{\pi(r_0^2 - r_i^2)} \tag{7}$$

where M_{sh} stands for the bed mass per unit height, r_i is the distance from the center to the surface of the expanded bed, ρ_s is the density of the solid particles and ε is the total bed void fraction. The total void fraction for a bed of solid micron size particles, as calculated by Eq. 7, is about 0.3 to 0.4 while the total void fraction for type APF agglomerates of nanoparticles is about 0.92 to 0.98. Therefore, the Darcy nondimensional number is of the order of several thousands for micron size particles so that the second term in Eq. 5 for the tangential velocity is negligible, whereas the Darcy number for a bed of agglomerates of nanoparticles is at least two orders of magnitude smaller (values from 10 to 60), so that the second term of Eq. 5 cannot be neglected.

It is important to note that we use the total void fraction of the bed in calculating the Darcy number; if the external fluidized bed void fraction (interagglomerate void fraction) were used instead, the Darcy number would be much higher, and of the same order as for micron sized particles (see Table 1). However, the very large internal porosity of the nanoagglomerates should affect the permeability κ, and is also an important factor (as discussed earlier) in determining the effective viscosity of the fluidized bed. For example, for agglomerates of nanoparticles which are 98 – 99% porous, even though their diameter is of the order of hundreds of microns, their mass or inertia is about two-orders of magnitude lower than of a solid micron particle of similar diameter. Hence, the effective viscosity of the fluidized bed will be much lower, reducing the Darcy number by about two-orders of magnitude, in addition to the reduction of the Darcy number due to the increase in permeability. The effective viscosity has not been considered in the calculations of the Darcy number in Table 1, and for this reason we used a total porosity, rather than the external void fraction, to account for the much lower effective viscosity.

Model that predicts a higher bed pressure drop

Our simulations using Fluent®, and the low effective viscosity of the bed due to the large total porosity of APF nanoagglomerates indicates that a large tangential velocity component within the flow pattern of the rotating fluidized bed (RFB) of APF powder may occur. Therefore, it is necessary to reformulate the problem using the Navier-Stokes for a steady axisymmetric, incompressible, nonlinear fluid flow through a bed of particles in a rotating cylindrical frame of reference[12]

$$R_o(\vec{u}\cdot\vec{\nabla})\vec{u} + 2(\vec{k}\times\vec{u}) = -\vec{\nabla}p + E_k\nabla^2\vec{u} - D\vec{u} - F|\vec{u}|\vec{u} \quad (8)$$

Equation 8 incorporates the nondimensional numbers R_o, E_k, D, and F, where D is the Darcy number and F is the Forcheimmer number. The Darcy and the Forcheimmer numbers appear in the equation due to the presence of the bed of particles;[12] the Darcy number has already been discussed in detail above, and the Forcheimmer number is given by

$$F = \frac{cU_o}{\Omega\sqrt{\kappa}} \quad (9)$$

where

$$c = 0.045\varepsilon^{-3/2} \quad (10)$$

and κ has been introduced in Eq. 6.

By assuming a fluidization particle diameter of 80 microns (either a nanoagglomerate or a solid particle), the nondimensional numbers (R_o, E_k, D, F) have been calculated based on our experimental conditions and are listed in Table 1. From this table, the Darcy number is the most relevant since the other nondimensional numbers are very small and can be neglected. Furthermore, the Darcy number is large when the porosity is low, that is, for solid micron size powders, and it is small when the porosity is large, that is, for a fluidized bed of agglomerates of nanoparticles. Considering the values of the nondimensional numbers, Eq. 8 can be simplified and reduced to

$$2(\vec{k}\times\vec{u}) = -\vec{\nabla}p \quad (11)$$

where p is the nondimensional pressure term that includes the centrifugal force as shown in Eq. 2.

By expanding Eq. 11, returning back to dimensional terms, simplifying and considering only the radial direction due to the axisymmetric flow, the following equation is obtained

$$\frac{1}{\rho}\frac{\nabla P}{\partial r}\,i_r = \Omega^2 r i_r + 2\Omega\cdot v_\theta i_r \quad (12)$$

This equation is applicable when fluidizing APF type agglomerates of nanoparticles, Aerosil® R974 and R972, at gas velocities higher than the minimum fluidization velocity. Equation 12 explains the higher experimental pressure drops observed than expected from models that do not consider tangential effects, that is, the Coriolis force.

In other words, as can be seen from Eq. 5, the fluidized agglomerates may have tangential velocities higher than the tangential velocity of the rotating frame (rigid body rotation); this means that the agglomerates may rotate at higher speeds than the rotating distributor due to gas entrainment in the tangential direction; therefore, the pressure drop across the bed can be increased due to the additional centrifugal acceleration.

In order to solve Eq. 12, a value for the tangential velocity has to be assumed. For example, considering a rotating frame of reference, the relative tangential velocity of the fluid can be found by subtracting the tangential velocity of the rotating frame of reference from the tangential velocity of the fluid obtained from a fixed frame of reference. As a first approximation, we assume a tangential velocity of the fluid to be equal to the distributor's tangential velocity. The actual tangential velocity of the fluid may in fact be larger as shown by the simulations in Figures 11 and 12; nevertheless, it can be seen that when the gas velocity at the inlet of the chamber is 6 m/s, the fluid velocity from the simulations can be approximated by the equation

$$v_\theta = \Omega R - \Omega r \quad (13)$$

Substituting this tangential velocity equation into Eq. 12 we obtain

$$\frac{1}{\rho}\frac{dP}{dr} = 2\Omega^2 R - \Omega^2 r \quad (14)$$

Equation 14 can be compared against the model of Kao et al.[10] for the fluidized bed pressure drop at gas velocities higher than the minimum fluidization velocity

$$\frac{dP}{dr} = (\rho_g - \rho_f)(1-\varepsilon)r\Omega^2 \quad \text{Kao et al.}[10] \quad (15a)$$

$$\frac{dP}{dr} = (\rho_g - \rho_f)(1-\varepsilon)(\Omega^2 r + 2\Omega\cdot v_\theta) \quad \text{This model} \quad (15b)$$

Our model, Eq. 15b, has an additional term due to the Coriolis force that represents the additional tangential effects that occur during fluidization of APF type powders.

By defining the distance from the fluidized bed surface to the center of the RFB as a fraction of the distributor's radius, "x," Eqs. 15a and 15b can be integrated according to the boundary conditions (P_1 at R_1, radius of the bed surface; P_2 at R, distributor's radius)

$$\Delta P = \rho_b\Omega^2\left(\frac{R^2}{2} - \frac{R_1^2}{2}\right) \quad (16a)$$

$$\Delta P = \rho_b\Omega^2\left[2R(R-R_1) - \left(\frac{R^2}{2} - \frac{R_1^2}{2}\right)\right] \quad (16b)$$

but

$$R_1 = xR \quad 0.5 < x < 1 \quad (17)$$

$$\Delta P = \frac{\rho_b\Omega^2 R^2}{2}(1-x^2) \quad (18a)$$

$$\Delta P = \frac{\rho_b\Omega^2 R^2}{2}(x^2 - 4x + 3) \quad (18b)$$

As can be seen, Eqs. 18a and 18b, which correspond to the model of Kao et al.[10] and our model, respectively, differ by a factor that depends on the fraction,. For example, if the surface of the fluidized bed is at 0.15 m from the center, for a fluid-

ized-bed height of 0.05 m, then. Hence, the pressure drop calculated with our model is 30% larger than the estimated by Kao et al.'s model. However, it should be noted that this assumption is based on a fluidized bed tangential velocity equal to the tangential velocity of the distributor, considering a fixed frame of reference. The actual tangential velocity may be even higher depending on the flow of air at the inlet of the chamber as seen by the simulations in Figures 11 and 12.

Prediction of agglomerate size by fractal analysis

Since data on bed expansion as a function of gas velocity is available for APF type agglomerates of nanoparticles, namely, Aerosil® R974 and Aerosil® R972, it is possible to apply the Richardson-Zaki approach coupled with a fractal model as applied by Nam et al.[5] and originally suggested by Valverde et al.[24]. Rotating fluidized bed expansion data for Aerosil® R972 was selected in order to estimate the agglomerate size and fluidized-bed void fraction.

The following equation is obtained when the Richardson-Zaki (R-Z) criterion is coupled with a fractal model[5]

$$\left(\mathrm{C}\frac{\mathrm{u}}{v_0}\right)^{(1/n)} = \mathrm{N}^{[1-(1/D_f)](1/n)}(1-\phi\mathrm{N}^{[(3/D_f)-1]}) \qquad (19)$$

where u is the gas velocity, C is the Cunningham correction factor which applies to particles less than 1 micron, ϕ is the total bed solid fraction (1-ε), v_0 is the settling velocity of a primary particle, n is the R-Z index (approximately five for low Reynolds number creeping flow),[25] N represents the number of primary particles in the agglomerate, and D_f corresponds to the fractal dimension. Since the values of u and can be obtained from the experimental data, Eq. 19 should yield a straight line with y-intercept and slope as explained by Nam et al.[5]

It is important to note that the settling velocity of the primary nanoparticle v_0, will be affected by the rotating speed of the frame since the settling velocity is dependent on the acceleration, as shown below

$$v_0 = \frac{2\mathrm{C}\rho_p r_p^2 G g}{9\mu} \qquad (20)$$

where the values for G come from the rotating speed of the distributor that simulates 10, 20, 30 or 40 times normal gravity acceleration g.

Figure 13 shows the straight lines from which the slope and the y-intercept can be obtained at 10 and 20 times normal gravity acceleration and the results are summarized in Table 2; unfortunately, there was not sufficient experimental data on bed expansion to obtain significant results at the higher rotating speeds. In plotting this figure, a Richardson-Zaki coefficient of 5 was used since the agglomerate Reynolds numbers for both

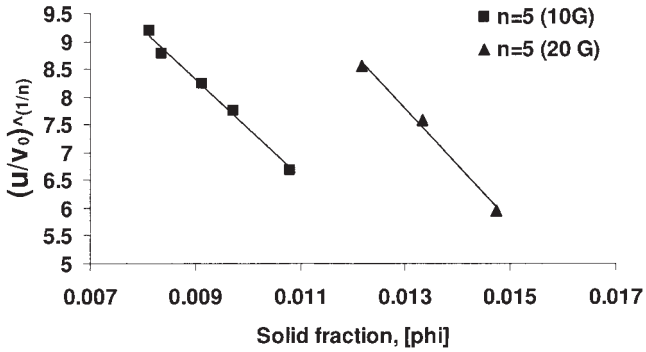

Figure 13. Plot of Eq. 19 for n = 5 at rotating speeds of 22 and 31 rad/s at 10 and 20 times normal gravity acceleration.

G = 10 and G = 20 were less than unity. The predicted size range for an agglomerate diameter at 211 rpm (G = 10) is around 120 microns, and the estimated agglomerate density is about 40 kg/m^3. The size of the agglomerate obtained by this method is smaller than the 160 microns size predicted for agglomerates during conventional fluidization.[5] Surprisingly, at the higher rotating speed of 300 rpm (G = 20), the size and density of the agglomerates increase to about 214 microns and 45 kg/m^3. This is contrary to the results reported by Masuda et al.[15], who calculated an agglomerate diameter (based on their model using their experimental measurements of the minimum fluidization velocity) that decreased with higher rotating speeds. However, for our APF nanoagglomerates, when the agglomerates are fluidizing under higher acceleration they get more compacted which is reflected in the larger calculated agglomerate density. In addition, at higher G the agglomerates are closer to one another because of a decrease in the bed void fraction reflected by a lower bed expansion at any given gas velocity (see Table 3).

The external or interagglomerate void fraction can also be calculated by this method and the results (along with the total bed void fractions) are given in Table 3, which shows that at any given gas velocity the external bed void fraction is lower at the higher rotating speed. Therefore, it is more likely for the agglomerates to collide with each other and to form larger agglomerates at 20 G than at 10 G. This may also explain the larger agglomerate size calculated at higher G. However, more research needs to be done to fully understand the effect of rotating speed on the average size of the nanoagglomerates during fluidization.

Concluding Remarks

Our experimental data show that it is possible to fluidize nanopowders in a rotating fluidized bed and different nanopowders show quite different behavior during fluidization. For

Table 2. Results from Applying the Richardson-Zaki Criterion Coupled with Fractal Analysis for $n = 5$

Gravity Force ($\times$9.8 m/s^2) G	Slope m	y-Intercept B	Agglomerate Diameter (μm)	Density of Agglomerate (kg/m^3)	Number of Particles N	Fractal Dimension Df
10	−891.0	16.3	120	40.4	9.3E+09	2.55
20	−1024.2	21.1	214	45.3	7.6E+10	2.55

Table 3. Comparison of the Radial Gas Velocity and the External Void Fraction around the Agglomerates (ε_x), Interagglomerate Void Fraction, at Different Rotating Speeds

22 rad/s = 10 G			31 rad/s = 20 G		
Superficial Radial Gas Velocity (m/s)	Total Void Fraction (ε)	Interagglomerate Void Fraction by *R-Z*-Fractal Analysis (ε_x)	Superficial Radial Gas Velocity (m/s)	Total Void Fraction (ε)	Interagglomerate Void Fraction by *R-Z*-Fractal Analysis (ε_x)
0.008	0.989	0.35	0.009	0.985	0.23
0.0168	0.990	0.41	0.03	0.986	0.31
0.0227	0.991	0.45	0.055	0.987	0.37
0.031	0.991	0.50			
0.039	0.992	0.51			

example, Aerosil® R974 and R972 fluidized with a significant bed expansion while Aeroxide® TiO_2 P25 did not show any appreciable bed expansion at all.

Some of the advantages of the rotating fluidized bed over conventional fluidization are: less elutriation of powder, fluidization at much higher gas velocities resulting in a much higher gas throughput per unit area of distributor, smaller footprint, thin beds resulting in either no bubbles or very small bubbles, very little gas bypassing and shorter time of processing. For example, the minimum fluidization velocity for Aerosil® R974 in conventional fluidization[4] is about 0.0025 m/s, while the minimum fluidization velocity of the same powder in a RFB at 10 times gravity acceleration is about 0.02 m/s, an order of magnitude higher.

Numerical simulations of the fluid flow pattern inside of a rotating cylinder show that the tangential velocity component is predominant over the radial component, and the hydrodynamics depend on the flow rate directed to the chamber, as well as the rotating speed of the distributor. The tangential velocity component of the fluid flow is very different from rigid body rotation which has been assumed in most of the previous literature references.

It has been found that the pressure drop of a fluidized bed of APF type agglomerates of nanoparticles is higher than that estimated using available mathematical models for RFBs. This phenomenon can be explained based on the existence of tangential momentum effects that arise because of the large porosity and reduced effective viscosity of the fluidized bed of agglomerates of nanoparticles. For these nanoagglomerates, estimating the bed pressure drop becomes difficult, and it depends not only on the centrifugal acceleration, but also on the fluidized bed expansion and tangential velocity component of the fluid bed. The tangential velocity component within the fluidized bed of APF type agglomerates of nanoparticles is significant in the expanded bed, that is, in the fluidized bed region close to the interface or bed surface, because the tangential velocity component from the empty geostropic region expands into the fluidized bed through the porous interface. The extension of the tangential flow into the fluidized bed is also promoted by its low effective viscosity, which results from the significant fluidized bed expansion of APF nanoparticles that increases the porosity of the bed.

Previous models on fluidization of solid micron size particles in a RFB, such as those formulated by Chen[11] and Kao et al.[10], neglected the Coriolis term in the fluid equation; these models gave reasonable results when compared with experiments where the effective viscosity was large, that is, large particles in beds of low porosity. Therefore, the tangential velocity within the fluidized beds was negligible, and only the radial component was important.

When the effective viscosity is small, however, it is believed that the tangential velocity component within the fluidized bed entrains the agglomerates in the direction of the flow, that is, tangentially. If this tangential velocity is larger than the tangential velocity of the rigid rotating frame, then the agglomerates are subject to an additional centrifugal acceleration that increases the fluidized-bed pressure drop.

The Richardson-Zaki criterion coupled with a fractal analysis can be used to approximate the agglomerate size and its density if enough data on fluidized-bed expansion is gathered. At 10 times normal gravity acceleration, this method predicted a smaller agglomerate size for a rotating fluidized bed when compared to a prediction of the agglomerate size for a conventional fluidized bed, a result that is reasonable. However, at 20 times normal gravity acceleration ($G = 20$), this method predicted an agglomerate size larger than at G = 10 in contrast to the results reported by Masuda et al.[15]. Further experiments at higher rotating speeds are clearly necessary to fully understand and elucidate the effect of rotating speed on the size of the nanoagglomerates formed during fluidization in a RFB.

Acknowledgments

We gratefully acknowledge the National Science Foundation for financial support through Grant No. DMI 0210400, NIRT - Collaborative Research: Experimental and Computational Investigations of Fluid Interactions/Transport in Nanodomains and Around Nanoparticles. Partial support from the New Jersey Commission on Science and Technology (No. 01-2042-007-24) is also acknowledged. We also thank the Degussa Corporation (U.S. and Japan) for providing us with the powders used in this study.

Notation

D = Darcy number, nondimensional
d_p = diameter of particle, m
Df = fractal dimension of an agglomerate
Ek = Ekman number, nondimensional
F = Forcheimmer number, nondimensional
g = gravitational acceleration, m/s^2
G = gravitational factor, nondimensional
M_{sh} = mass per length of expanded bed, kg/m
n = Richardson-Zaki exponent
N = number of primary particles in an agglomerate
Re = Reynolds number, nondimensional
Ro = Rossby number, nondimensional
r_o = distributor radius, m
r_i = distance from the interface (gas-solid) to the center, m

u = superficial gas velocity, m/s
U = gas velocity, m/s
Ug = fluidization velocity, m/s
U_{mf} = minimum fluidization velocity, m/s
Vr = radial gas velocity, m/s
$V\theta$ = tangential velocity, m/s

Greek letters

ε = void fraction, nondimensional
κ = permeability constant, m^2
μ_f = fluid viscosity, $(N.s/m^2)$
ϕ = volume fraction of primary particles in the bed
ρ_a = density of agglomerate, kg/m^3
ρ = gas density, kg/m^3
ρp = particle density, kg/m^3
δ = distance between two particles, nm
Ω = rotating speed, rad/s

Literature Cited

1. Watano S, Imada Y, Hamada K, Wakamatsu Y, Tanabe Y, Dave R, Pfeffer R. Microgranulation of fine powders by a novel rotating fluidized bed granulator. *Powder Technol*. 2003;131:250-255.
2. Watano S, Nakamura H, Hamada K, Wakamatsu Y, Tanabe Y, Dave R, Pfeffer R. Fine particle coating by a novel rotating fluidized bed coater. *Powder Technol*. 2004;141:172-176.
3. Qian G, Bagyi I, Burdick I, Pfeffer R, Shaw H, Stevens J. Gas-solid fluidization in a centrifugal field. *AIChE J*. 2001;47:1022-1033.
4. Zhu C, Yu Q, Pfeffer R, Dave R. Gas fluidization characteristics of nanoparticle agglomerates. *AIChE J*. 2005;51-2:426-439.
5. Nam C, Pfeffer R, Dave R, Sundaresan S. Aerated vibrofluidization of silica nanoparticles. *AIChE J*. 2004;50:1776-1785.
6. Zhu C, Liu G, Yu Q, Pfeffer R, Dave R, Nam C. Sound assisted fluidization of nanoparticle agglomerates. *Powder Technol*. 2004;141: 119-123.
7. Yu Q, Dave R, Zhu C, Quevedo J, Pfeffer R. Enhanced fluidization of nanoparticles in an oscillating magnetic field. *AIChE J*. 2005;51:1971-1979.
8. Wang Y, Wei F, Jin Y, Luo T. Agglomerate particulate fluidization and e-particles. *Proceedings of CUChE-3*. Beijing: Tsinghua University Press; 2000.
9. Kroger DG, Levy EK, Chen JC. Flow characteristics in packed and fluidized rotating beds. *Powder Technol*. 1979; 24:9-18.
10. Kao J, Pfeffer R, Tardos GI. On partial fluidization in rotating fluidized beds. *AIChE J*. 1987;33:858-861.
11. Chen YM. Fundamentals of a centrifugal fluidized bed. AIChE Journal.1987; 33:722-728.
12. Arman B. *Fluid mechanics of flow through rotating cylinders with and without packed media*. Bethlehem: Lehigh University; 1989. Doctoral dissertation.
13. Watano S, Imada Y, Hamada K, Wakamatsu Y, Tanabe Y, Dave R, Pfeffer R. Microgranulation of fine powders by a novel rotating fluidized bed granulator. *Powder Technol*. 2003;131:250-255.
14. Saunders JH. Particle entrainment from rotating fluidized beds. *Powder Technol*. 1986;47:211-217.
15. Matsuda S, Hatano H, Muramoto T, Tsutsumi A. Modeling for size reduction of agglomerates in nanoparticle fluidization. *AIChE J*. 2004; 50:2763-2771
16. Wen CY, Yu YH. A generalilzed method for predicting the minimum fluidization velocity. *AIChE J*. 1966;12:610.
17. Wang Y, Gu G, Wei F, Wu J. Fluidization and agglomerate structure of SiO_2 nanoparticles. *Powder Technol*. 2002;124:152-159.
18. Vanyo JP. *Rotating Fluids in Engineering and Science*. New York: Dover Publications; 2001.
19. Zhu C, Lin CH, Qian GH, Pfeffer R. Modeling of the pressure drop and flow field in a rotating fluidized bed. *6th World Congress of Chemical Engineering*, Melbourne: Australia; 2001.
20. Bennetts DA, Jackson DN. Source-sink flows in a rotating annulus: a combined laboratory and numerical study. *J Fluid Mechanics*. 1974; 66:689-705.
21. Kunii D, Levenspiel O. *Fluidization engineering*. New York: Wiley; 1969.
22. Zhao Y, Wei L. Rheology of gas-solid fluidized bed. Fuel Processing Technology. 2000; 68:153-160.
23. Poletto M, Joseph D. The effective density and viscosity of a suspension. *J Rheology*. 1995;39(2): 323-343.
24. Valverde J, Quintanilla M, Castellanos A, Mills P. The settling of fine cohesive powders. *Europhysics Letts*. 2001;54:329-334
25. Richardson JF, Zaki, WN. Sedimentation and Fluidisation: Part I. *Trans Instn Chem Engrs.* 1954;32:35-53.

Manuscript received Sept. 22, 2005, and revision received Feb. 8, 2006.